On stress drop, cohesion and seismogenic index of fluid-induced seismicity

Serge A. Shapiro[1] and Carsten Dinske[2]

[1]Freie Universität Berlin
[2]Freie Universität Berlin

November 24, 2022

Abstract

A significant stress drop characterizes sometimes earthquakes induced by injection or extraction of fluids in rocks. Moreover, long-term fluid operations in underground reservoirs can impact a seismogenic reaction of the rocks per a unit volume of the involved fluid. The seismogenic index is a quantitative characteristic of such a reaction. We derive a relationship between the seismogenic index and the stress drop. We propose a simple and rather general phenomenological model of the stress drop of induced events in various faulting regimes. Our results suggest that high stress drops of some earthquakes induced by long-term underground fluid operations may be controlled by drops of cohesion of more cohesive faults getting seismically activated due to gradually increasing with time differential stresses. On the one hand, this effect can result in an increase of seismogenic index with production time. On the other hand, a production-caused depleting of the pore pressure can also cause a systematic increase of the stress drop. This provides an additional contribution to the growth of seismogenic index with production time at such reservoirs.

On stress drop, cohesion and seismogenic index of fluid-induced seismicity

S. A. Shapiro[1], **C. Dinske**[1]

[1]Freie Universität Berlin, Earth Science Department, Section of Geophysics, Malteserstrasse 74-100, Building D, 12249 Berlin, Germany

Key Points:

- We derive a relation between the stress drop and the seismogenic index of induced seismicity
- We derive a simple and rather general phenomenological model of stress drop in various faulting regimes
- Rupture-related drop of fault cohesion may control high stress drop of some events induced by long-term reservoir developments

Corresponding author: Serge Shapiro, `shapiro@geophysik.fu-berlin.de`

Abstract

A significant stress drop characterizes sometimes earthquakes induced by injection or extraction of fluids in rocks. Moreover, long-term fluid operations in underground reservoirs can impact a seismogenic reaction of the rocks per a unit volume of the involved fluid. The seismogenic index is a quantitative characteristic of such a reaction. We derive a relationship between the seismogenic index and the stress drop. We propose a simple and rather general phenomenological model of the stress drop of induced events in various faulting regimes. Our results suggest that high stress drops of some earthquakes induced by long-term underground fluid operations may be controlled by drops of cohesion of more cohesive faults getting seismically activated due to gradually increasing with time differential stresses. On the one hand, this effect can result in an increase of seismogenic index with production time. On the other hand, a production-caused depleting of the pore pressure can also cause a systematic increase of the stress drop. This provides an additional contribution to the growth of seismogenic index with production time at such reservoirs.

1 Introduction

Stress drop is a change in the shear stress produced by the earthquake on its rupture surface. It is an important parameter characterizing the earthquake physics (e.g., (Shearer, 2009), (R. E. Abercrombie et al., 2016)). Thus, there is a large number of detailed interesting and important works dedicated to this parameter. Unfortunately, any kind of a representative reviewing of them is beyond the scope of this paper. Below we refer to several such selected publications to indicate tendencies significant to our further consideration.

Stress drop is of practical importance. It can influence ground motions in engineering-relevant frequency domains (e.g., (Boore, 1983), (Hough, 2015), (Huang et al., 2017)). In this respect, stress drop of induced earthquakes can be of especial interest. There are observations indicating that the average stress drop of induced seismicity is lower than the one of tectonic events (e.g., (R. Abercrombie & Leary, 1993), (Hough, 2015)). However, there are publications indicating that induced and tectonic events do not show principal differences in stress drops (e.g., (Huang et al., 2017), (Zhang et al., 2016), (Clerc et al., 2016), (Goertz-Allmann et al., 2011), (Tomic et al., 2009)). Moreover, (Goertz-Allmann et al., 2011) and (Huang et al., 2017) observe indications of systematic stress drop dependencies on the pore pressure and on the hypocenter depths, respectively.

Frequently, stress drop estimates are based on computing corner frequencies of displacement spectra of earthquake wavefields. (Shapiro et al., 2013) proposed another approach for estimating average stress drop of seismicity induced in a finite rock volume. This estimate is based on a fitting of the so-called lower-bound of the magnitude probability to the magnitude frequency distribution of induced seismicity. For various case studies of induced seismicity, they obtained average stress drop estimates in a very broad range of 10^2 to 10^7 Pa (see also our Table 1). Such values do not contradict conclusions of (Huang et al., 2017) and (Goertz-Allmann et al., 2011) that stress drop of induced seismicity is controlled by in-situ tectonic stresses and in-situ pore pressures. However, some very low values of stress drop may indicate a specific physics of induced events in some case studies.

Intuitively, in the shallow sedimentary structures (up to 3-4 km depth), one would not expect production-induced events with a high stress drop. However, sometimes a significant stress drop is observed by hydrocarbon production induced seismicity. For example, Maury et al., (1992) observed stress drops approximately up to 4 MPa at the Lacq field, in France. Groningen gas field (the Netherlands) is another recent example of the production-induced seismicity (Bourne et al. 2014, Bommer et al. 2016, Dost et al. 2016, Grigoli et al, 2017). The seismicity at the Groningen field is related to the reservoir pres-

sure depletion resulting in compaction and subsidence of the free surface. Dost and Bommer (2016) show results for some events at Groningen indicating stress drop values reaching up to 10 MPa. Also the lower-bound-based average stress drop estimate is in the same order (Shapiro et al, 2017). Moreover, (Bourne et al., 2018) show that the production induced seismicity of Groningen is characterized by a systematic increase of event number per unit volume of the extracted gas. This observation is also supported by increasing with time estimates of the seismogenic index at the Groningen field (Shapiro, 2018).

What is the reason of high stress drop values sometimes observed in shallow sediments? What is the reason of the growth of the seismogenic index with production time? Are these observations mutually related? In this paper we show that these features of the long-term production induced seismicity are possibly mutually related. We show that an averaged stress drop is closely related to the seismogenic index. Then we derive a rather general model of the stress drop. This model is applicable to the induced seismicity in various tectonic regimes. This model is in agreement with the observed tendencies indicating a load (depth) impact on stress drops, ((Huang et al., 2017), and (Goertz-Allmann et al., 2011)). Then we discuss additional factors controlling stress drop. We conclude that high stress drops of some earthquakes induced by long-term underground fluid operations may be controlled by drops of cohesion of more cohesive faults which are getting gradually seismically activated through the fluid extractions or injections.

2 Seismogenic index and the stress drop

We start with recalling the definition of the seismogenic index. It is frequently observed that the rate of the fluid-injection induced seismicity is controlled by the rate of the injected fluid mass (Shapiro et al. 2007, Ellsworth, 2013, McGarr 2014, Langenbruch and Zoback, 2016, Shirzaei et al. 2016). The seismogenic index model of (Shapiro et al., 2010, 2007) (see also chapter 5 of (Shapiro, 2015) for more details) provides an equation describing these observations under rather realistic conditions of a monotonic (non-decreasing) injection pressure, and approximately point-like independent induced earthquakes in a homogeneous porous continuum. For a nearly incompressible injection fluid, like water, the rate of injected fluid mass is proportional to the volumetric flow rate. The corresponding equation describes the cumulative number of events $N_{\geq M}(t)$ with moment magnitudes larger than M which occurred until the time t elapsed since the injection start (Shapiro et al. 2007, 2010, Shapiro, 2015, 2018):

$$\lg N_{\geq M}(t) = \Sigma + \lg Q_{fluid}(t) - bM, \tag{1}$$

where $\lg \equiv \log_{10}$ (we accept this notation everywhere in this paper), b is the b-value of the Gutenberg-Richter magnitude frequency statistic: $\lg N_{\geq M} = a - bM$ ((Gutenberg & Richter, 1954)). Further, $Q_{fluid} = Q_{inj}(t)$ is the fluid volume injected until time t elapsed after beginning of fluid operations and Σ is the seismogenic index of the rock volume stimulated by the injection. We accept the system SI of physical units (thus, the fluid volume must be measured in cubic meters). Equation (1) can be used for estimation of the seismogenic index Σ from seismicity observations.

The theory of the seismogenic index model (1) is based on the assumption that the seismicity is triggered by pore-fluid pressure perturbations (or failure stress changes directly related to an increase of the fluid mass at the hypocenter of an event). Equation (1) is obtained by a combination of the Gutenberg-Richter magnitude probability law with an integral of the pore pressure perturbation in the stimulated volume. Then, equation (1) is a direct consequence of the fluid mass conservation law for a nearly incompressible injection fluid.

Shapiro (2018) generalized the seismogenic index model to poroelastic coupling processes involved in the triggering of seismicity by fluid productions or injections. The

seismogenic index can be represented as follows:

$$\Sigma = \Sigma_0 + \delta\Sigma, \tag{2}$$

where Σ_0 is a reference value of the seismogenic index characterizing a potential seismogenic reaction of an infinite fluid-saturated statistically homogeneous medium with a given level of seismo-tectonic activity on a unite volume of the injected fluid in the case of seismicity triggering by increasing pore pressure. The quantity $\delta\Sigma$ describes deviations of the seismogenic index from its reference value due to specific boundary and initial conditions, poroelastic coupling and other mechanisms and factors impacting the seismicity triggering process.

Using equation (2), Shapiro (2018) shows that, in the case of a fluid production equation (1) is still valid. However, $Q_{fluid}(t)$ is given by a re-scaled volume of the fluid produced until the time t elapsed after production start. This volume should be expressed in cubic meters of the in-situ fluid saturating the pore space in the reservoir: $Q_{fluid}(t) = Q_{prod}(t)\rho_{prod}/\rho_{in-situ}$, where $Q_{prod}(t)$ is the real volume of the produced fluid at normal conditions, ρ_{prod} is its density at normal conditions, and $\rho_{in-situ}$ is the density of the fluid saturating the reservoir pore space in-situ. Estimates of Σ obtained from equation (1) without correcting for this density effect and without accounting for $\delta\Sigma$ of equation (2) can be understood as apparent or effective values of Σ. They still can be used to infer the fluid-induced seismicity under assumptions of nearly stationary or slowly changing reservoir characteristics. In the last case Σ should be additionally extrapolated to account for temporal trends.

Figure 1 shows how model (1) does describe the number of events (with magnitudes larger than the completeness one, M_w 1.5) induced by the gas production in the Groningen gas field in the period of years 1993-2016. (the seismicity and production data are respectively taken from https://www.knmi.nl/kennis-en-datacentrum/dataset/aardbevingscatalogus and https://www.nam.nl/algemeen/mediatheek-en-downloads/winningsplan-2016.html). More details on the seismicity catalogs can be found, e.g., in works of (Dost et al., 2016), (Bommer et al., 2016) and further sources referred to in these publications. Equation (1) corresponds to the set of straight dotted lines plotted for values of Σ increasing with a step of 0.25 from a lower to an upper one, consequently. The model provides low estimates of the reference seismogenic index Σ_0 in the range of -6 to -4 (see for more details Shapiro, 2018). Dinske and Shapiro (2013) estimated the seismogenic index in several regions. They observed values varying from -10 (very low seismogenic activity) to 1 (very high seismogenic activity). The values of Groningen indicate a tectonic regime with a rather low seismogenic activity. However, Figure 1 indicates that the seismogenic index at Groningen has a tendency to gradually increase with time. This is also in agreement with the estimates made by Shapiro (2018), who shown that this increasing tendency of Σ is statistically significant. Moreover, this tendency is in agreement with the observations of (Bourne et al., 2018) that the seismicity rate normalized to the rate of the reservoir volume change is increasing with time. To some extend the increasing seismogenic index at Groningen can be related to a changing density of the in-situ fluid due to a production-related depleting pore pressure. Below, we propose two effects potentially contributing predominantly to the physics of this observation.

Theoretically, the reference value Σ_0 of the seismogenic index is equal to the logarithm of the product of the following four factors ((Shapiro et al., 2010; Shapiro, 2015)): (i) volume concentration of the potential point-like defects, N (e.g., cracks where microearthquakes can occur); (ii) the probability of an event with a positive magnitude, 10^{a_w}; (iii) an average probability density of the pore pressure perturbation necessary to trigger events, $1/C_{max}$; and (iv) a reciprocal uniaxial storage coefficient of the rock, $1/S$.

$$\Sigma_0 = a_w + \lg \frac{N}{C_{max} S}. \tag{3}$$

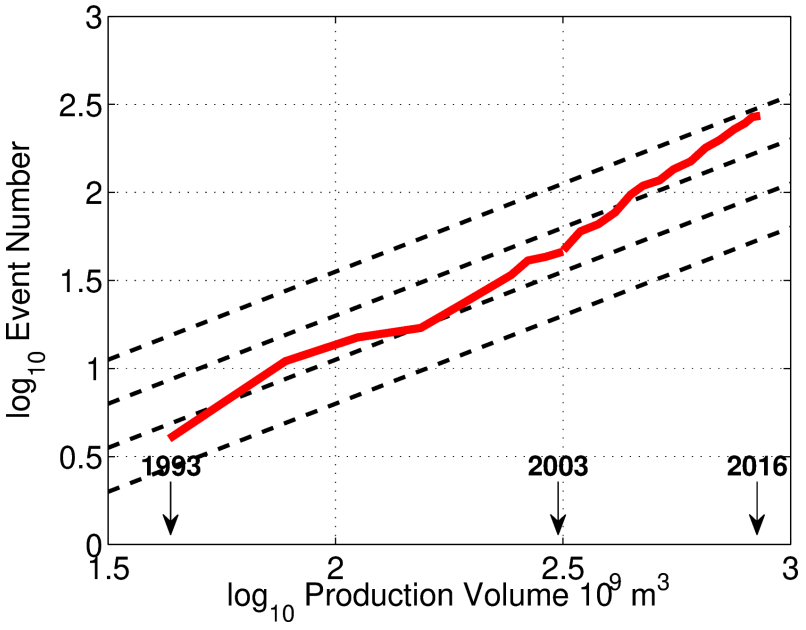

Figure 1. Cumulative number of seismic events as a function of the produced gas volume in Groningen field in the periods of 1993-2016. The set of straight dotted lines is given by equation (1) with values of Σ consequently increasing with a step of 0.25 from a lower to an upper line, respectively.

A relation between the seismogenic index and the stress drop follows from the relation between Σ_0 and the probability of positive moment magnitudes. Following Shapiro et al. (2013), in order to work in the frame of the Gutenberg-Richter magnitude distribution, we assume a power-law probability density function (PDF) f_X for the size distribution of potential rupture surfaces with length X in an infinite rock volume (see also Section 5.2 of Shapiro, 2015):

$$f_X = A_X X^{-q}, \tag{4}$$

with A_X a proportionality constant and exponent q numerically related to the Gutenberg-Richter b value, $q = 2b + 1$, characterizing the statistic of potential earthquake with these rupture surfaces. A power-law type of statistic is characteristic for hierarchical heterogeneous systems of fractal nature ((Mandelbrot, 1983)). It is frequently assumed for describing properties of fault systems ((Turcotte, 1997)). Strictly, it is assumed that such a power-law PDF is an approximation of a real PDF of sizes of potential rupture surfaces in the length domain above a certain minimum characteristic size X_{min} (which is probably comparable to a pore scale of rocks). In general, the integral of the PDF over all possible sizes X must be equal to 1. From this condition we obtain, $A_X = 2bX_{min}^{2b}$. A known relation between the rupture size X and the moment magnitude $M = \lg[X^2\Delta\sigma/\kappa_0]^{3/2} - 6.07$ ((Shearer, 2009), (Lay & Wallace, 1995), (Kanamori & Brodsky, 2004)) can be used then to derive an equation for the a_w value of the Gutenberg-Richter magnitude probability. Equation (37) of (Shapiro et al., 2013) provides a_w:

$$a_w = \lg\left[X_{min}^{2b}\int_0^\infty f_C(C_\sigma)C_\sigma^{-2b}dC_\sigma\right]. \tag{5}$$

$f_C(C_\sigma)$ is the probability density of C_σ which is a quantity proportional to the cubic root of reciprocal stress drop, $C_\sigma \approx 1084\kappa_0^{1/3}/\Delta\sigma^{1/3}$ where κ_0 is a rupture-shape related undimensional constant in the order of 1, and the stress drop $\Delta\sigma$ is measured in Pascals. The

integral above represents an ensemble averaging of the quantity C_σ^{-2b}. Thus,

$$a_w = \lg\left[X_{min}^{2b}\langle C_\sigma^{-2b}\rangle\right] \approx \lg\left[\frac{X_{min}}{1084C^{1/3}}\right]^{2b} + \lg\langle\Delta\sigma^{2b/3}\rangle. \quad (6)$$

If the PDF of the stress drop is very broad and flat representing a nearly uniform distribution between a very low $\Delta\sigma_{min}$ and a very high $\Delta\sigma_{max}$, then $\langle\Delta\sigma^{2b/3}\rangle \propto \Delta\sigma_{max}^{2b/3}$. If the stress drop PDF is like a δ-function, we will obtain $\langle\Delta\sigma^{2b/3}\rangle \approx \Delta\sigma^{2b/3}$. In both cases the following relation is approximately valid:

$$\Sigma_0 \approx \frac{2b}{3}\lg\langle\Delta\sigma\rangle + 2b\lg\frac{X_{min}}{1000} + \lg\frac{N}{C_{max}S}. \quad (7)$$

The second and third terms on the right-hand side of this equation are stress-drop independent quantities. Finally, if stress drop is characterized by a log-normal PDF (as frequently assumed, e.g., Goertz-Allmann et al., 2011), then $\langle\Delta\sigma^{2b/3}\rangle = \langle\Delta\sigma\rangle^{2b/3}\exp(b(2b-3)\sigma_x^2/9)$ and a fourth nearly constant small term should be added to the right hand part. This term is in the order of $0.05\sigma_x^2$, where σ_x^2 is a variance of $\ln[\Delta\sigma/\langle\Delta\sigma\rangle]$. According to equation (7), we expect a rather loose but linear proportionality between the logarithm of stress drop and seismogenic index with a proportionality coefficient $\frac{2}{3}b$.

This observation is consistent with a range of seismogenic index and stress drop estimates shown in Figure 2. The crosses in this Figure represent pairs of values of average stress drops and seismogenic indices computed for various case studies of induced seismicity (i.e., one pair of values per a case study). These estimates were obtained by a fitting of the so-called lower-bound statistic (which is given by a finite size of a stimulated rock volume) to the observed magnitude-frequency distributions (see for more details (Shapiro et al., 2011), (Shapiro et al., 2013) and (Shapiro, 2015), Chapter 5). An averaged stress drop can be computed using a characteristic size of the stimulated volume (approximately corresponding to the stimulated-volume minimum principal scale limiting the rupture propagation) and using an estimate of the maximum induced magnitude (which is a fitting parameter of the lower-bound statistic curve). The estimates of the seismogenic index were obtained for corresponding case studies using their frequency-magnitude distributions, injected fluid volumes and equation (1). Their values are given in Table 1. The Figure shows also a line with a slope that corresponds to $b = 1$. Although the number of data points is small, their distribution indicates indeed the linear proportionality given by equation (7).

As mentioned above, at the Groningen gas field, the seismogenic index seems to be increasing with time. Equation (7) suggests that it can be explained by an increasing with time averaged stress drop (see also our argumentation in the Discussion). In addition, Figure 2 indicates that the stress drop values in the order of 1 to 10 MPa seem to be too high for the seismogenic index in the range of -6 to -4 as observed in Groningen ((Shapiro, 2018)). Regular values of the stress drop should be significantly below 1 MPa. What can explain high stress drop events at Groningen? What can cause the increasing with time stress drop? In the next section we propose a rather general analytic model of the stress drop in various faulting regimes. Using this model further in the Discussion, we address these two questions.

3 Stress drop vs effective stress

Here we provide a simple and rather general phenomenological consideration attempting to constrain the stress drop of a seismic event occurred under a normal-, thrust- or strike slip tectonic faulting regime. We accept a Mohr-Coulomb framework and assume that at the moment of an earthquake stop, the dynamic friction (which is smaller than the static one) exceeds the shear stress on the earthquake fault. Further, we assume that earthquake-caused changes in the vertical stress are small and they contribute only

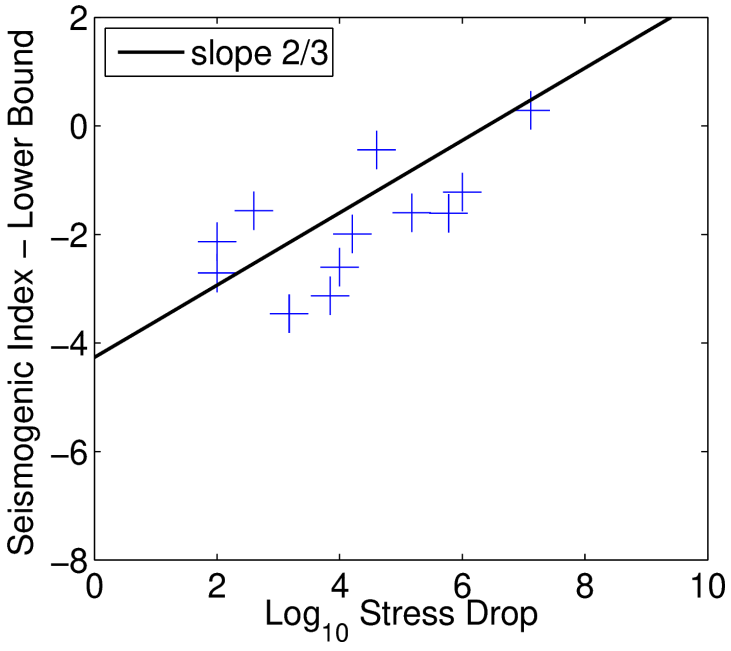

Figure 2. Seismogenic index versus static stress drop (Pa) for various case studies of fluid-injection induced seismicity. The Figure is based on estimates of the stress drop and of the seismogenic index given in (Dinske and Shapiro, 2013) and (Shapiro et al., 2013). Modified from (Dinske and Shapiro, 2017)

insignificantly to the stress drop. This should be especially the case for small-magnitude induced earthquakes in sedimentary rocks characterized by weak elastic heterogeneity in lateral directions. In such rocks, the vertical stress is given by the load of a layered approximately 1-D heterogeneous overburden. Thus, we assume that the earthquake does not change the vertical stress (at least, its average on the fault plane remains approximately unchanged). Equally, we assume that the rupture caused dilatation effects on the pore pressure are small. At least for moderate deformations below 10^{-3}–10^{-2} they should be several orders of magnitude smaller than the hydrostatic pressure, and this is sufficiently small to neglect them for our consideration below. This should be especially the case for induced seismicity in highly porous permeable reservoir rocks. Further, we assume that the earthquake fault orientation is unchanged as well. We do not consider here the physics of the friction coefficient. We just assume, that due to the rupture process it suffers some changes. Effects like the rate and state dependent friction evolution could be included for a modeling of these changes. However, such type of modeling remains beyond the frame of our consideration.

We start with a normal faulting regime. We consider an earthquake fault initially being just in a critical state. Thus, the angle between the fault plane and the largest principal stress (under the normal faulting, it is the vertical stress, σ_v; compressive principal stresses are positive in this paper) is equal to $0.25\pi - 0.5\phi_0$, where ϕ_0 is the static friction angle (a friction angle is denoted by a double arc on Figure 3a). From the assumptions above we can compute the differential stress $\sigma_d^{(n)}$ (the index (n) here and in the following denotes the normal faulting stress regime). It is equal to the diameter of the critical Mohr-Coulomb circle (see Figure 3a):

$$\sigma_d^{(n)} = 2\frac{C_0 \cos\phi_0 + (\sigma_v - P_p)\sin\phi_0}{1 + \sin\phi_0}, \tag{8}$$

where C_0 is the cohesion and P_p is the pore pressure. Then, the critical shear stress $\tau_c^{(n)}$ on the earthquake fault under static friction is given by the following expression:

$$\tau_c^{(n)} = [C_0 + (\sigma_v - P_p)\tan\phi_0](1 - \sin\phi_0), \tag{9}$$

Further, on a plane making an arbitrary angle $\theta < \pi/4$ to the main stress direction, the shear stress is:

$$\tau^{(n)}(\theta) = \frac{[C_0\cos\phi_0 + (\sigma_v - P_p)\sin\phi_0]\sin(2\theta)}{1 + \sin\phi_0}, \tag{10}$$

During the earthquake the friction force is governed by a dynamic friction coefficient $\tan\phi$ with a friction angle ϕ. This new friction coefficient and the vertical stress define a new critical Mohr-Coulomb circle (see Figure 3b). The shear stress on the earthquake fault, $\tau_e^{(n)}$, will be reduced. It can be computed using equation (10) and substituting $\theta = 0.25\pi - 0.5\phi_0$ (the fault orientation remains unchanged) and the dynamic friction coefficient instead of the static one:

$$\tau_e^{(n)} = [C + (\sigma_v - P_p)\tan\phi]\frac{\cos(\phi)\cos(\phi_0)}{1 + \sin\phi}, \tag{11}$$

where we have also accounted for a possibility of a rupturing-cased cohesion changing from C_0 to C. Therefore, the stress drop $\Delta\sigma^{(n)} = \tau_c^{(n)} - \tau_e^{(n)}$ reads:

$$\Delta\sigma^{(n)} = [C_0 + (\sigma_v - P_p)\tan\phi_0](1 - \sin\phi_0) - [C + (\sigma_v - P_p)\tan\phi]\frac{\cos(\phi)\cos(\phi_0)}{1 + \sin\phi}. \tag{12}$$

Assuming a vanishing cohesion on earthquake faults ($C_0 = C = 0$) and a small difference $\Delta\mu_f$ between the static and dynamic friction coefficient we arrive to the following approximation of the stress drop:

$$\Delta\sigma_0^{(n)} \approx -\Delta\mu_f(\sigma_v - P_p)(1 - \sin\phi_0)^2. \tag{13}$$

Here and in the following the index 0 of the stress drop denotes the assumption of initially zero-cohesion faults. Please note that a reduction of the friction coefficient leads to a positive stress drop proportional to the main effective stress. For example, $\mu_f = 0.6$ and $-\Delta\mu_f \leq 0.1$ provides

$$\Delta\sigma_0^{(n)} \leq 0.024(\sigma_v - P_p). \tag{14}$$

For example, for the depth of 3km and a hydrostatic pore pressure we obtain $\Delta\sigma^{(n)}$ in the order of 1.1 MPa or less.

Further, we consider a thrust faulting regime. We accept the same assumptions. However now, the vertical stress is the minimum principal stress (see Figure 3c). From the assumptions formulated above we can compute the differential stress, which is equal to the diameter of the critical Mohr-Coulomb circle (see Figure 3 a and c):

$$\sigma_d^{(t)} = 2\frac{C_0\cos\phi_0 + (\sigma_v - P_p)\sin\phi_0}{1 - \sin\phi_0}. \tag{15}$$

On the earthquake fault under static friction, the critical shear stress is given then by the following expression:

$$\tau_c^{(t)} = [C_0 + (\sigma_v - P_p)\tan\phi_0](1 + \sin\phi_0), \tag{16}$$

On a plane making an arbitrary angle $\theta < \pi/4$ with the main stress direction, the shear stress is:

$$\tau^{(t)}(\theta) = \frac{[C_0\cos\phi_0 + (\sigma_v - P_p)\sin\phi_0]\sin(2\theta)}{1 - \sin\phi_0}, \tag{17}$$

On the earthquake fault, the shear stress, $\tau_e^{(t)}$, will be reduced. It can be computed using equation (17) and substituting $\theta = 0.25\pi - 0.5\phi_0$. Also, the dynamic friction coefficient must be substituted instead of the static one:

$$\tau_e^{(t)} = [C + (\sigma_v - P_p)\tan\phi]\frac{\cos(\phi)\cos(\phi_0)}{1-\sin\phi}. \tag{18}$$

Therefore, the stress drop $\Delta\sigma^{(t)} = \tau_c^{(t)} - \tau_e^{(t)}$ is:

$$\Delta\sigma^{(t)} = [C_0 + (\sigma_v - P_p)\tan\phi_0](1+\sin\phi_0) - [C + (\sigma_v - P_p)\tan\phi]\frac{\cos(\phi)\cos(\phi_0)}{1-\sin\phi}. \tag{19}$$

Assuming a vanishing cohesion on earthquake faults and a small difference between the static and dynamic friction coefficient we arrive to the following approximation of the stress drop:

$$\Delta\sigma_0^{(t)} \approx -\Delta\mu_f(\sigma_v - P_p)(1+\sin\phi_0)^2. \tag{20}$$

Interestingly, this consideration predicts that under equivalent effective vertical stress, in the case of small friction coefficients, the difference between stress drops under thrust and normal faulting regimes is insignificant. However, in the case of usual values of friction coefficients the stress drop of thrust events is approximately one order of magnitude higher. Indeed, let us assume $\mu_f = 0.6$ and $-\Delta\mu \leq 0.1$. This provides (compare this result to eq. 13):

$$\Delta\sigma_0^{(t)} \leq 0.23(\sigma_v - P_p). \tag{21}$$

For example, for the depth of 3km and a hydrostatic pore pressure we obtain the stress drop in the order of 10MPa or less.

Let us finally consider a strike-slip faulting regime. We accept the same assumptions as above. However, the vertical stress is not any more important for our derivation. Instead we will firstly assume that we know the initial effective mean stress, $\sigma_{m0} - P_p$ (it is the center of the Mohr-Coulomb circle on Figure 3a). Firstly we compute the differential stress which is equal to the diameter of the critical Mohr-Coulomb circle:

$$\sigma_d^{(s)} = 2[C_0\cos\phi_0 + (\sigma_{m0} - P_p)\sin\phi_0]. \tag{22}$$

On the earthquake fault under static friction, the critical shear stress is given then by the following expression:

$$\tau_c^{(s)} = [C_0 + (\sigma_{m0} - P_p)\tan\phi_0]\cos^2\phi_0, \tag{23}$$

On a plane making an arbitrary angle $\theta < \pi/4$ to the main stress direction, the shear stress is:

$$\tau^{(s)}(\theta) = [C_0 + (\sigma_{m0} - P_p)\tan\phi_0]\cos\phi_0\sin(2\theta), \tag{24}$$

On the earthquake fault, the shear stress, $\tau_e^{(s)}$, will be reduced. It can be computed using equation (24) and substituting $\theta = 0.25\pi - 0.5\phi_0$ and the dynamic friction coefficient instead of the static one:

$$\tau_e^{(s)} = [C + (\sigma_m - P_p)\tan\phi]\cos(\phi)\cos(\phi_0). \tag{25}$$

Therefore, the stress drop $\Delta\sigma^{(s)} = \tau_c^{(s)} - \tau_e^{(s)}$ reads:

$$\Delta\sigma^{(s)} = [C_0 + (\sigma_{m0} - P_p)\tan\phi_0]\cos^2\phi_0 - [C + (\sigma_m - P_p)\tan\phi]\cos(\phi)\cos(\phi_0). \tag{26}$$

Assuming a vanishing cohesion on earthquake faults, approximately unchanged during rupture mean stress and a small difference between the static and dynamic friction coefficient we arrive to the following approximation of the stress drop:

$$\Delta\sigma_0^{(s)} \approx -\Delta\mu_f(\sigma_{m0} - P_p)(1-\sin^2\phi_0). \tag{27}$$

Thus, if we approximate σ_{m0} by σ_v we conclude that this stress drop is between the ones of normal and thrust faulting earthquakes. For example, let us assume $\sigma_{m0} \approx \sigma_v$ (at least they must be in the same order), $\mu_f = 0.6$ and $-\Delta\mu \leq 0.1$. This provides

$$\Delta\sigma_0^{(s)} \leq 0.074(\sigma_v - P_p). \tag{28}$$

For example, for the depth of 3km and a hydrostatic pore pressure we obtain the stress drop in the order of 3.3 MPa or less.

Above we have estimated stress drops of events rupturing nearly optimally oriented faults. They are representative for the order of maximum expected stress-drop values of induced seismicity. Equation (13) shows that we indeed can expect increasing stress drops with a depletion of the pore pressure. However in the normal faulting regime, it provides rather small stress drops. In the next section we discuss this aspect.

4 Discussion

Above we derived simple approximations of the stress drop (equations (13), (14), (20), (21) and (27), (28)) under the assumption of zero-cohesion faults. This is a reasonable assumption for a long-term tectonic active fault systems. Let us consider another situation. We assume that an earthquake has been induced on a preexisting originally passive and cohesive fault. We hypothesize that the cohesion is reduced to zero during the earthquake. Indeed, the cohesion is related to the uniaxial tensile strength of faults (Jaeger et al., 2007). One can expect that this strength reduces significantly or it vanishes after an earthquake. Then, the orders of maximum expectations of the stress drop in normal-, thrust- and strike-slip regimes will be given by complete equations (12), (19) and (26) with $C_0 > 0$ and $C = 0$. Respectively, these estimates are:

$$\Delta\sigma_c^{(n)} \approx [C_0 - \Delta\mu_f(\sigma_v - P_p)(1 - \sin\phi_0)](1 - \sin\phi_0). \tag{29}$$

$$\Delta\sigma_c^{(t)} \approx [C_0 - \Delta\mu_f(\sigma_v - P_p)(1 + \sin\phi_0)](1 + \sin\phi_0). \tag{30}$$

$$\Delta\sigma_c^{(s)} \approx [C_0 - \Delta\mu_f(\sigma_v - P_p)]\cos^2\phi_0. \tag{31}$$

These estimates will be very strongly influenced by the maximum cohesion change equal to initial cohesion C_0. At shallow depths, small variations of the friction coefficient contribute to the stress drop significantly less. Assuming usual values $\mu_f = 0.6$, $\Delta\mu_f = -0.1$, $C_0 = 10MPa$, the depth of 3km and a hydrostatic pore pressure we obtain the following estimates of the maximum expected stress drop in normal-, thrust- and strike slip regimes, respectively: 6 MPa, 25 MPa and 10.5 MPa. Thus even in the case of normal faulting (like the Groningen gas field where the absolute majority of estimated fault plane solutions of events shows the normal faulting as demonstrated by (Willacy et al., 2018), (Willacy et al., 2019)), relatively high stress drop values can be observed. They should correspond to events occurring on initially cohesive faults.

Moreover, our equations (29)-(31) show that the stress drop will increase with a depletion of the pore pressure systematically (see the terms with the effective vertical stress). Correspondingly, equation (7) suggests that the seismogenic index will increase systematically as well. On the right-hand side of this equation the first term is directly dependent on the stress drop. Two other terms depend on structural-, elastic- and general tectonic properties of the geological setting. They should not be characterized by a significant production-time dependence. Under this assumption, equation (7) provides the following result for a change of the seismogenic index due to a long-term production:

$$\Sigma_0(t_2) - \Sigma_0(t_1) \approx \frac{2b}{3}\lg\frac{\langle\Delta\sigma(t_2)\rangle}{\langle\Delta\sigma(t_1)\rangle} \approx \frac{2b}{3}\lg\frac{C_2 - \Delta\mu_f(\sigma_v - P_p(t_2)(1 - \sin\phi_0)}{C_1 - \Delta\mu_f(\sigma_v - P_p(t_1))(1 - \sin\phi_0)}, \tag{32}$$

where we denoted by t_1 and t_2 two time moments of the production history $t_1 < t_2$ and, C_1 and C_2 represent averaged cohesion of faults getting seismogenic at t_1 and t_2, respectively. The second part of the right-hand side of this equation is written for the normal

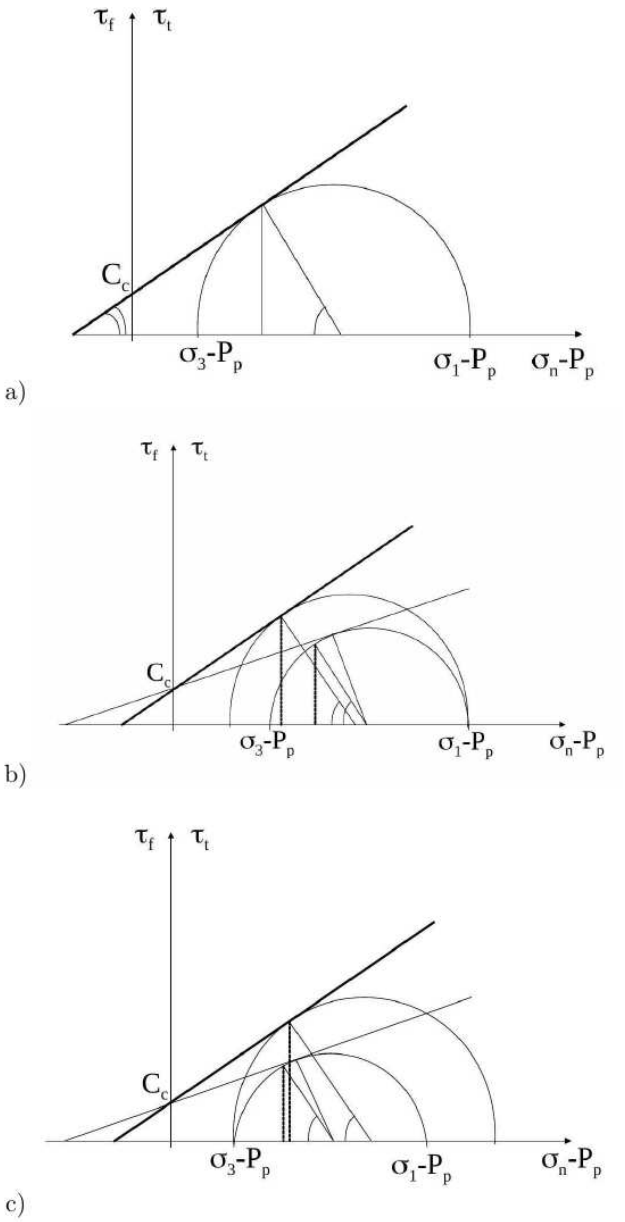

Figure 3. A sketch for the stress drop computation. Figure 3a shows the Mohr-Coulomb plot of the shear stress as a function of the effective normal stress on a fault plane (the semi-circle). The thick straight line describes the friction resistance of faults. The contact point of this line with the circle corresponds to the critically stressed fault plane ready for an earthquake. Figure 3b corresponds to a normal faulting regime. In addition to Figure 3a it shows the Mohr-Coulomb circle (the smaller one) immediately after the termination of the rupture process. Also a dynamic friction straight line is shown here. It is shown here for exactly the same cohesion C_c as the static friction line. However, this must not be necessarily the case. It is possible, that before the earthquake $C_c = C_0$ and after the earthquake C_c accepts another (logically, lower) value $C_c = C$ (see the text). The two vertical lines show shear stresses on the earthquake fault before and after the rupture process. Figure 3c is exactly the same as Figure 3b, but for a thrust faulting regime.

faulting regime. Let us make estimates realistic for the situation at Groningen. We consider two time moments separated by a long production period, e.g., 10 years. We assume typical values of $\sigma_v = 75MPa$, $P_p(t_1) = 30MPa$, $P_p(t_2) = 15MPa$. Thus, a partial systematic increase in the seismogenic index will be due to a systematic depletion of the pore pressure. It is expressed by the $P_p(t)$ dependence in equation (32). Another part of this increase can be related to the following effect. Due to the poroelastic coupling the decreasing pore pressure causes an increase of the differential stress. Indeed, in the normal faulting regime, the increase of the differential stress is proportional to the decrease of the pore pressure (see e.g., Shapiro, 2018). Therefore, the Mohr-Coulomb circle on Figure 3a will grow with time. Thus gradually with the production time, the Mohr-Coulomb circle will start to touch failure envelopes characterized by higher values of the cohesion C. In other words, faults with higher values of cohesion will be gradually involved into the seismogenic process. This can lead to an increase of an average initial cohesion of faults producing earthquakes at later time periods. To estimate a contribution order of this effect we assume a minimum value $C_1 = 0$ and a realistically high value $C_2 = 5MPa$. Further, as previously, we assume $\Delta\mu_f = -0.1$ and $\mu_f = 0.6$. The common contribution of the both effects mentioned above is given by equation (32). It provides $\Sigma_0(t_2) - \Sigma_0(t_1) \approx 0.4$. This level of changes of the seismogenic index is indeed observed at Groningen (see Shapiro, 2018 and our Figure 1). This is also in agreement with the observations of exponentially increasing with time seismicity (Borne et al., 2018).

Therefore, the estimates above show that a long term fluid production from a normal-faulting reservoir can lead to a time-dependent seismogenic index. This time dependence is relatively weak (of a logarithmic type, e.g., 0.4 in 10 years, in a situation like Groningen gas field) and can be rather simply taken into account. Thus, the seismogenic index model will be still appropriate to infer the fluid-induced seismicity from the produced fluid volume. Interestingly, a production from a normal-faulting Groningen type of reservoirs reduces the absolute value of horizontal stresses (see e.g., Shapiro, 2018). This leads to a stabilization of the normal-faulting regime. A long term production from a reservoir with a strike-slip or trust-faulting tectonic can theoretically change the type of the faulting regime (by reducing the horizontal stresses due to the poroelastic coupling). Such a dramatic change of the faulting tectonic should be visible on the temporal behavior of the reservoir's seismogenic index. Thus, Σ becomes an important monitoring quantity able to provide useful information about an evolution of the seismo-tectonic state of the reservoir. For example, a growing Σ may indicate an increasing with time maximum possible magnitude, M_{max}.

In spite of a set of assumption we accepted for our estimates of the stress drop, we hypothesize that because these assumptions are rather realistic and not very specific, our analytic results have a general character at least as order-of-magnitude estimates. These estimates do not clearly provide a reason of a principal difference of stress drops of induced and tectonic events. On the one hand, they indicate that stress drops of events on cohesion-less faults should show some increasing with depth tendency. This is similar to the observations of (Goertz-Allmann et al., 2011) and (Huang et al., 2017) indicating effective stress dependencies of the stress drop. However analogously to the conclusions of (Huang et al., 2017), these dependencies are similar to the tendencies of shear strengths of cohesion-less faults. On the other hand, if the average stress drop of a set of seismic events is mainly defined by the drop of cohesion of involved faults, then depth dependencies can become invisible. As previously mentioned, there are observations of relatively low stress drops of induced seismicity (e.g., (R. Abercrombie & Leary, 1993), (Hough, 2015), see also our Figure 2). They could correspond to situations where the seismicity occurs on cohesion-less faults with very low shear strengths.

Finally, our stress-drop model shows that, another stress-drop controlling factor is a change of the friction coefficient $\Delta\mu_f$. We assumed a constant absolute value of it

Table 1. Stress drop $\Delta\sigma$ and seismogenic index Σ. for various case studies. The values of the quantities are colected from (Dinske & Shapiro, 2013), (Dinske & Shapiro, 2017), (Shapiro et al., 2013)

Seismicity catalog	$\Delta\sigma$ $[kPa]$	Σ
Soultz 1993 (EGS, crystalline)	0.4	-1.56
Soultz 1995 (EGS, crystalline)	0.1	-2.71
Soultz 1996 (EGS, crystalline)	0.1	-2.13
Soultz 2000 (EGS, crystalline)	40	-0.44
Basel (EGS, crystalline)	13000	0.29
Paradox Valley (Saltwater disposal, carbonate)	10	-2.60
Cotton Valley tight sand (gas)	7	-3.13
	16	-1.99
	2	-3.46
Horn River shale (gas)	600	-1.61
	1600	-1.22
	150	-1.60

in the order of 0.1. However, we cannot exclude that the evolution of the friction coefficient of induced events may have a specific physics distinguished from this one of tectonic earthquakes. This is an interesting subject for further research.

5 Conclusions

We have considered a relation between the stress drop and the seismogenic index. The case study of Groningen gas field provides interesting information in this respect. A significant stress drop of some induced earthquakes at Groningen can be explained by activating pre-existing cohesive normally-stressed fault systems. Seismic events on such faults lead to the drop of their cohesion due to the rupture process. This cohesion drop contributes directly to the earthquake stress drop. The production-related increase of the differential stress in the reservoir leads to an increasing number of seismically activated more cohesive faults. This leads in turn to an increasing seismogenic index.

The seismogenic index seems to be quite low at Groningen. However, it increases systematically with the production time. One of reasons of this behavior can be related to the average cohesion of involved faults as it is mentioned above. An additional effect contributing to this increase is a systematically increasing stress drop due to the production-related pressure depletion increasing the effective stress in the reservoir. A growing seismogenic index may may result in an increasing with time maximum possible magnitude, M_{max}.

Acknowledgments

This is a theoretical and modeling paper. There is no data necessary to understand, evaluate, or replicate our results. Careful and detailed reviews of the Associate Editor and of the Reviewer helped us to strongly improve the manuscript. We thank the sponsors of the *PHASE university consortium project* for supporting the research presented in this paper.

References

Abercrombie, R., & Leary, P. (1993). Source parameters of small earthquakes recorded at 2.5 km depth, cajon pass, southern california: implications for earthquake scaling. *Geophysical Research Letters*, *20*(14), 1511–1514.

Abercrombie, R. E., Bannister, S., Ristau, J., & Doser, D. (2016). Variability of earthquake stress drop in a subduction setting, the hikurangi margin, new zealand. *Geophysical Journal International*, ggw393.

Bommer, J., Dost, B., Edwards, B., Stafford, P., van, E. J., Doornhof, D., & Ntinalexis, M. (2016). Developing an application-specific ground-motion model for induced seismicity. *Bulletin of the Seismological Society of America*, *106*, 158–173. Retrieved from `http://dx.doi.org/10.1785/0120150184` doi: 10.1785/0120150184

Boore, D. M. (1983). Stochastic simulation of high-frequency ground motions based on seismological models of the radiated spectra. *Bulletin of the Seismological Society of America*, *73*(6A), 1865–1894.

Bourne, S. J., Oates, S. J., & van Elk, J. (2018). The exponential rise of induced seismicity with increasing stress levels in the groningen gas field and its implications for controlling seismic risk. *Geophysical Journal International*, *213*(3), 1693-1700. Retrieved from `http://dx.doi.org/10.1093/gji/ggy084` doi: 10.1093/gji/ggy084

Bourne, S. J., Oates, S. J., van Elk, J., & Doornhof, D. (2014). A seismological model for earthquakes induced by fluid extraction from a subsurface reservoir. *Journal of Geophysical Research: Solid Earth*, *119*(12), 8991–9015. Retrieved from `http://dx.doi.org/10.1002/2014JB011663` (2014JB011663) doi: 10.1002/2014JB011663

Clerc, F., Harrington, R. M., Liu, Y., & Gu, Y. J. (2016). Stress drop estimates and hypocenter relocations of induced seismicity near crooked lake, alberta. *Geophysical Research Letters*, *43*(13), 6942–6951.

Dinske, C., & Shapiro, S. (2013). Seismotectonic state of reservoirs inferred from magnitude distributions of fluid-induced seismicity. *J. Seismology*, *17*, 13-25, doi:10.1007/s10950-012-9292-9.

Dinske, C., & Shapiro, S. (2017). Scaling of injection-induced earthquake magnitude statistic and implications for seismic hazard assessment. In *Physics and Application of Seismic Emission. PHASE Research Project. Annual Report 2016.*

Dost, B., Edwards, B., & Bommer, J. (2016). *Local and moment magnitudes in the Groningen field* (Tech. Rep.). NAM. Retrieved from `http://feitenencijfers.namplatform.nl/download/rapport/62253e3b48434e65aa8b6d5186cc00df?open=true`

Dost, B., Edwards, B., & Bommer, J. J. (2018). The Relationship between M and ML: A Review and Application to Induced Seismicity in the Groningen Gas Field, The Netherlands. *Seismological Research Letters*, *89*(3), 1062–1074.

Ellsworth, W. L. (2013). Injection-induced earthquakes. *Science*, *341*, 1225942.

Goertz-Allmann, B. P., Goertz, A., & Wiemer, S. (2011). Stress drop variations of induced earthquakes at the basel geothermal site. *Geophysical Research Letters*, *38*(9).

Grigoli, F., Cesca, S., Priolo, E., Rinaldi, A. P., Clinton, J. F., Stabile, T. A., ... Dahm, T. (2017). Current challenges in monitoring, discrimination, and management of induced seismicity related to underground industrial activities: A european perspective. *Reviews of Geophysics*, *55*(2), 310–340. Retrieved from `http://dx.doi.org/10.1002/2016RG000542` (2016RG000542) doi: 10.1002/2016RG000542

Gutenberg, B., & Richter, C. F. (1954). *Seismicity of Earth and associated phenomenon.* Princeton: Princeton University Press.

Hough, S. E. (2015). Shaking intensity from injection-induced versus tectonic earthquakes in the central-eastern united states. *The Leading Edge*, *34*(6),

690–697.

Huang, Y., Ellsworth, W. L., & Beroza, G. C. (2017). Stress drops of induced and tectonic earthquakes in the central united states are indistinguishable. *Science advances*, *3*(8), e1700772.

Jaeger, J. C., Cook, N. G. W., & Zimmerman, R. W. (2007). *Fundamentals of rock mechanics*. Blackwell Publishing.

Kanamori, H., & Brodsky, E. E. (2004). The physics of earthquakes. *Rep. Prog. Phys.*, *67*, 1429–1496.

Langenbruch, C., & Zoback, M. D. (2016). How will induced seismicity in Oklahoma respond to decreased saltwater injection rates? *Science Advances*, *2*(11), e1601542, DOI: 10.1126/sciadv.1601542.

Lay, T., & Wallace, T. C. (1995). *Modern Global Seismology*. Academic Press.

Mandelbrot, B. B. (1983). *The fractal geometry of nature* (Vol. 173). WH freeman New York.

Maury, V., Grassob, J.-R., & Wittlinger, G. (1992). Monitoring of subsidence and induced seismicity in the lacq gas field (france): The consequences on gas production and field operation. *Engineering Geology*, *32*(3), 123–135.

McGarr, A. (2014). Maximum magnitude earthquakes induced by fluid injection. *J. Geophys. Res. Solid Earth*, *119*, 1008–1019, doi:10.1002/2013JB010597.

Shapiro, S. A. (2015). *Fluid-Induced Seismicity*. Cambridge: Cambridge University Press.

Shapiro, S. A. (2018). Seismogenic index of underground fluid injections and productions. *Journal of Geophysical Research: Solid Earth*, *123*(9), 7983–7997.

Shapiro, S. A., Dinske, C., & Krueger, O. (2017). Maximum magnitudes of earthquakes induced by fluid injections and productions: Controlling parameters, estimations, and case study examples. In *2017 seg international exposition and annual meeting* (pp. SEG-2017-17630886, 4pp).

Shapiro, S. A., Dinske, C., & Kummerow, J. (2007). Probability of a given-magnitude earthquake induced by a fluid injection. *Geophysical Research Letters*, *34*, L22314, doi:10.1029/2007GL031615.

Shapiro, S. A., Dinske, C., Langenbruch, C., & Wenzel, F. (2010). Seismogenic index and magnitude probability of earthquakes induced during reservoir fluid stimulations. *The Leading Edge*, *29*(3), 304–309, doi:10.1190/1.3353727.

Shapiro, S. A., Krüger, O. S., & Dinske, C. (2013). Probability of inducing given-magnitude earthquakes by perturbing finite volumes of rocks. *Journal of Geophysical Research: Solid Earth*, *118*(7), 3557–3575, doi:10.1002/jgrb.50264.

Shapiro, S. A., Krüger, O. S., Dinske, C., & Langenbruch, C. (2011). Magnitudes of induced earthquakes and geometric scales of fluid-stimulated rock volumes. *Geophysics*, *76*, WC53–WC61, doi:10.1190/GEO2010-0349.1.

Shearer, P. M. (2009). *Introduction to seismology*. Cambridge: Cambridge University Press.

Shirzaei, M., Ellsworth, W. L., Tiampo, K. F., González, P. J., & Manga, M. (2016). Surface uplift and time-dependent seismic hazard due to fluid injection in eastern texas. *Science*, *353*(6306), 1416–1419. Retrieved from `http://science.sciencemag.org/content/353/6306/1416` doi: 10.1126/science.aag0262

Tomic, J., Abercrombie, R., & Do Nascimento, A. (2009). Source parameters and rupture velocity of small m 2.1 reservoir induced earthquakes. *Geophysical Journal International*, *179*(2), 1013–1023.

Turcotte, D. L. (1997). *Fractals and chaos in geology and geophysics*. Cambridge university press.

Willacy, C., van Dedem, E., Minisini, S., Li, J., Blokland, J. W., Das, I., & Droujinine, A. (2018). Application of full-waveform event location and moment-tensor inversion for groningen induced seismicity. *The Leading Edge*, *37*(2), 92–99.

Willacy, C., van Dedem, E., Minisini, S., Li, J., Blokland, J.-W., Das, I., & Droujinine, A. (2019). Full-waveform event location and moment tensor inversion for induced seismicity. *Geophysics*, *84*(2), KS39–KS57.

Zhang, H., Eaton, D. W., Li, G., Liu, Y., & Harrington, R. M. (2016). Discriminating induced seismicity from natural earthquakes using moment tensors and source spectra. *Journal of Geophysical Research: Solid Earth*, *121*(2), 972–993.

Figure_1.

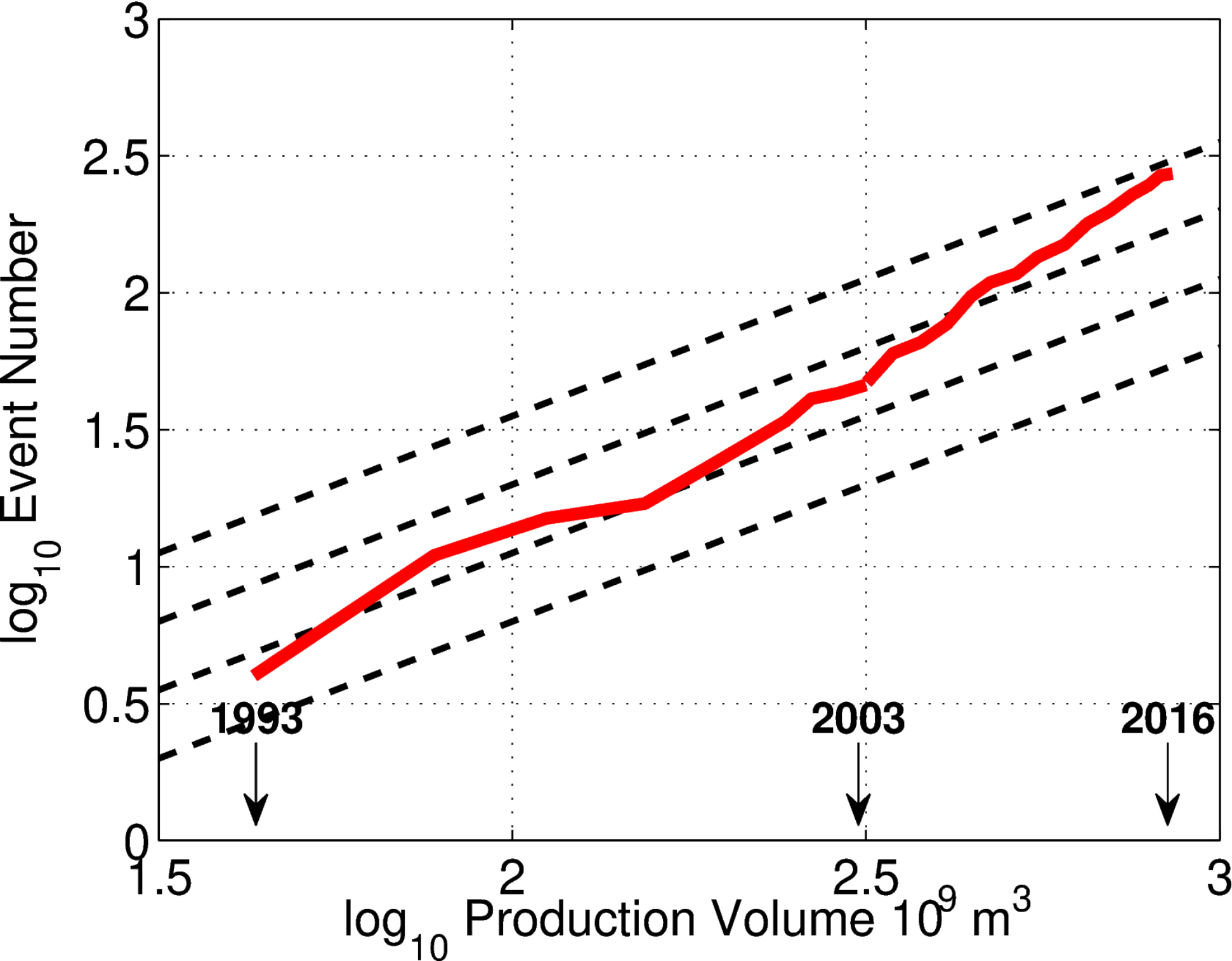
3
2.5
2
1.5
1
0.5
0
log10 Event Number
1993
2003
2016
1.5
2
2.5
3
log10 Production Volume 10^9 m^3

Figure_2.

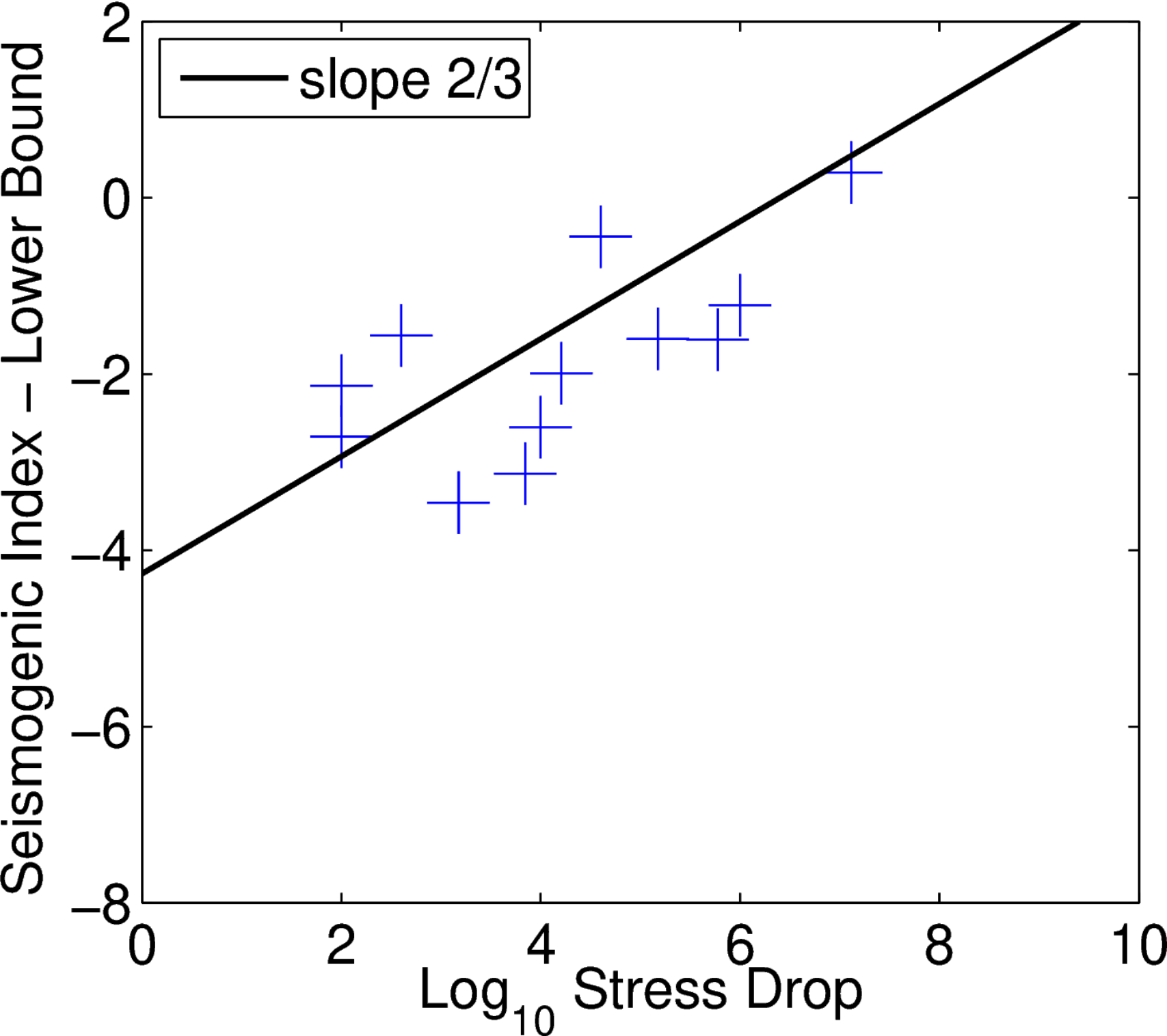
slope 2/3
Seismogenic Index – Lower Bound
Log10 Stress Drop
2
0
−2
−4
−6
−8
0
2
4
6
8
10

Figure_3.

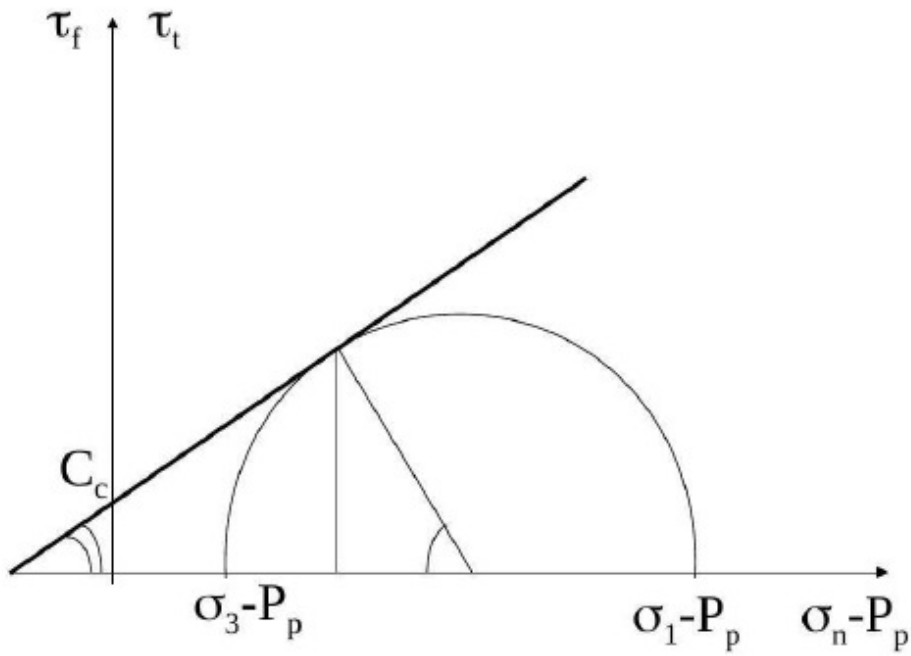
τf
τt
Cc
σ3-Pp
σ1-Pp
σn-Pp

a)

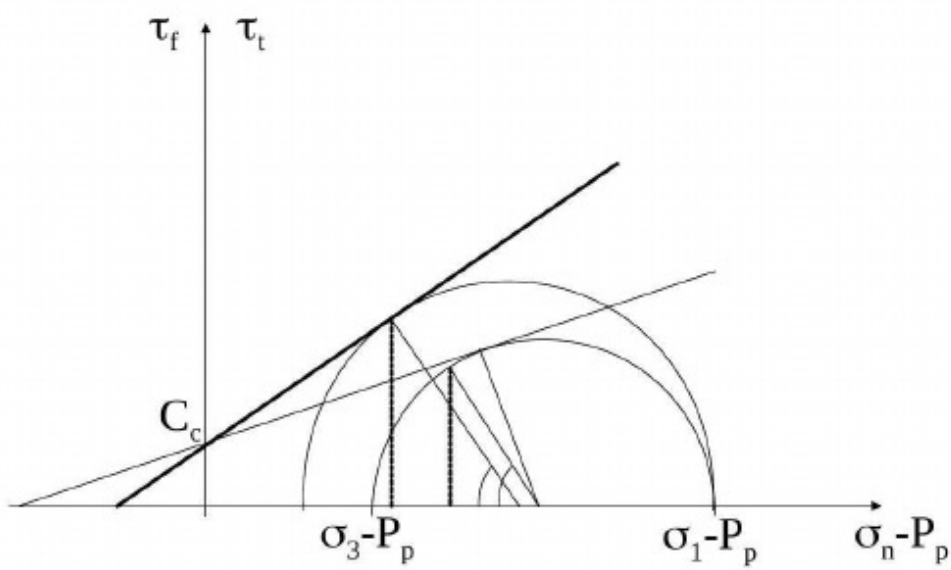
τf
τt
Cc
σ3-Pp
σ1-Pp
σn-Pp

b)

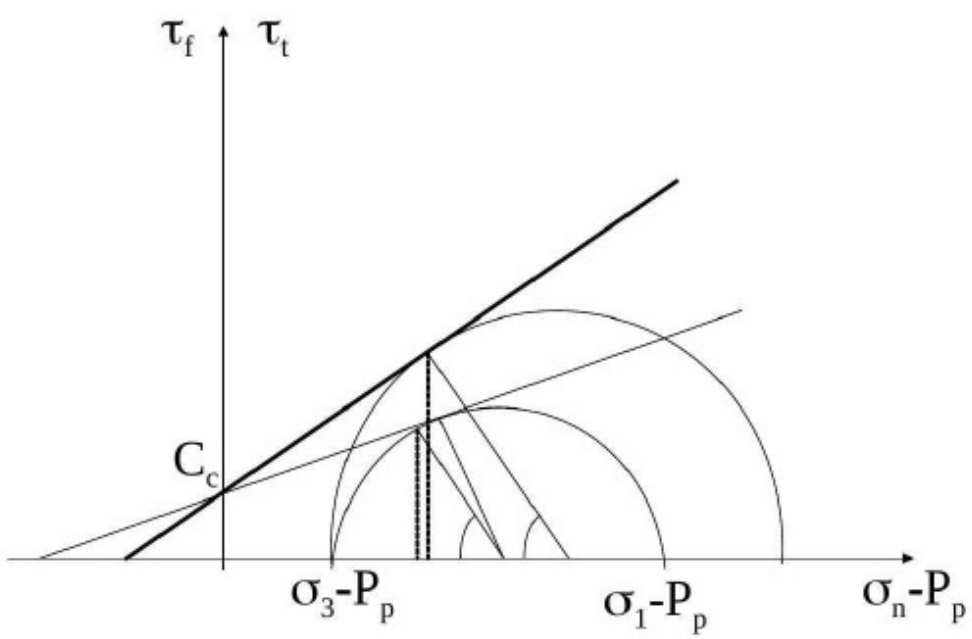
τf
τt
Cc
σ3-Pp
σ1-Pp
σn-Pp

c)